JOURNAL OF GEOPHYSICAL RESEARCH, VOL. 99, NO. D8, PAGES 16,557–16,567, AUGUST 20, 1994

Measurements of N_2O fluxes from fertilized grassland using a fast response tunable diode laser spectrometer

F. G. Wienhold, H. Frahm, and G. W. Harris[1]

Air Chemistry Department, Max Planck Institute for Chemistry, Mainz, Germany

Abstract. A fast response tunable diode laser spectrometer was used to make N_2O flux measurements by both eddy correlation and concentration gradient techniques during a methods intercomparison field program in April 1992 at a site in Stirling, Scotland. A description of the site and the results of the intercomparison are presented in companion papers. Sufficient instrumental precision and time resolution for N_2O flux determination using both techniques were obtained by application of the recently developed two-tone frequency modulation coupled with fast scanning of the laser. The use of a dedicated digital signal processor allowed zero-overhead on-line data handling at a rate of 10 Hz such that the time response of the system was only limited by the gas exchange time in the multipass sample cell (200 ms). Vertical concentration gradients that lead to a difference of ≤ 1 part per billion by volume in the N_2O mixing ratio at 0.06- and 1.05-m elevation were statistically resolved within 1 min. Eddy correlation measurements with intake heights of 2.25 m and 2.75 m were made in conjunction with two different sonic anemometers. The software developed for reduction and analysis of the 10-Hz eddy correlation data was based on time efficient FFT methods and performed time-base matching of the data set, drift correction, coordinate rotation, and evaluation of the covariances and the frequency power distributions. N_2O fluxes determined with this technique were in the range of 38–113 ng N m^{-2} s^{-1}. An unusual shape of the N_2O concentration covariance function can be ascribed to fetch inhomogeneities, and we conclude that the eddy correlation data set contains information that can be used to characterize the spatial variability in N_2O emission in addition to its spatial integral.

1. Introduction

Nitrous oxide mixing ratios are increasing in the global troposphere at a rate of $\approx 0.2\%$ per year [*Intergovernmental Panel on Climate Change (IPCC),* 1990], and although the reasons for this increase are presently not fully understood, it is generally accepted that the largest source of atmospheric N_2O originates in natural soil processes or activities related to land use [*Robertson,* 1993]. Quantitative relationships between soil properties and other environmental factors and actual N_2O emission rates are at present not sufficiently well understood to permit modeling of emissions over extended regions or time frames, which is an essential task in understanding the global N_2O budget. Many studies have demonstrated a high degree of spatial and temporal variability in N_2O fluxes, leading to an urgent need for techniques which allow determination of average fluxes over areas much larger than those normally studied by cover box methods. The micrometeorological method of eddy correlation flux determination [*Fowler and Duyzer,* 1989] has the potential to yield average values of N_2O fluxes over intermediate scales (10^3 to 10^4 m^2) which are very valuable for extrapolation to regional scales. However, the requirements for precision and response speed placed on the gas sensor by the eddy correlation method are stringent. We report here the design and performance of a novel laser spectrometer which meets these requirements and its first application in a field study of N_2O fluxes from fertilized grassland. Full details of the measurement site and the results of an intercomparison of various flux measurement techniques are given in companion papers [*Smith et al.,* this issue; *Clayton et al.,* this issue; *Hargreaves et al.,* this issue].

2. Sampling Arrangement

The experimental setup during the intercomparison campaign is illustrated in Figure 1. In order not to perturb the wind field, the intake section was mounted on a scaffold 15 m upwind from the van containing the tunable diode laser absorption spectrometer (TDLAS) and the associated equipment. Flow disturbance was minimal, as we verified in the data analysis (coordinate rotation angles, see paragraph 5). Using a three-way valve (V1), the inlet system could be switched between gradient and eddy correlation mode. In

[1] Now at Centre for Atmospheric Chemistry, York University, North York, Ontario, Canada.

Copyright 1994 by the American Geophysical Union.

Paper number 93JD03279.
0148-0227/94/93JD-03279$05.00

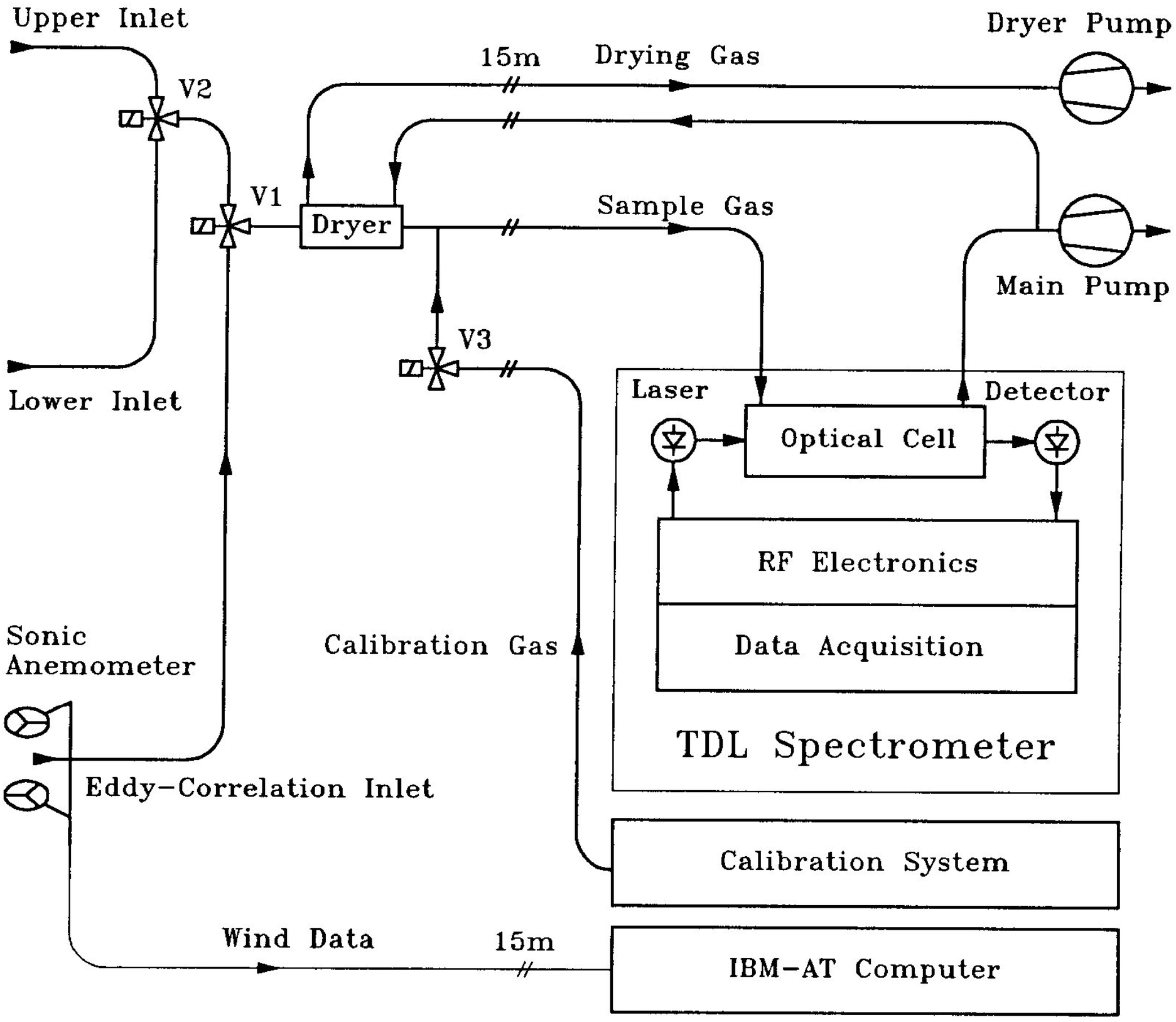

Figure 1. Setup of the tunable diode laser experiment during the Stirling intercomparison campaign. The inlet system (left) was mounted on a scaffolding 15 m upwind from the measurement van containing the spectrometer and associated equipment (right).

gradient mode, a solenoid valve (V2) driven by the TDLAS data acquisition computer toggled between two inlets at different heights (0.06 m and 1.05 m above ground), while for the eddy correlation measurements a third inlet conducted the air sampled in the vicinity of the sonic anemometer directly into the rest of the intake section. This section consisted of a Perma Pure multitube dryer (two stages model PD–1000–24), another solenoid valve (V3), which allowed the system to be purged with calibration or zero gas, and a 100 slm MKS mass flow controller for pressure reduction. The pressure in the optical cell was maintained constant at 50 mbar ($\pm <$ 1 mbar). The pressure drop of a few hundred millibar across the 15 m 1/2" tube (0.9-cm inner diameter) between the scaffolding and the van caused a fast turbulent flow. From Figure 2, which shows the response of the system after ambient air was suddenly replaced by N_2 at the inlet point, a transfer time of 0.7 s can be deduced. The flow velocity was 24.3 m/s, and the Reynolds number was 16,200. According to *Lenshow and Raupach* [1991] the attenuation of concentration fluctuations in the tube was characterized by a cutoff frequency of 5.4 Hz under these conditions, so that the overall time response was determined only by the measurement cell gas exchange time (200 ms), as can also be seen from Figure 2.

To avoid the need for density corrections due to water vapor and heat fluctuations [*Webb et al.,* 1980], the air was dried and equilibrated to constant temperature before entering the optical cell. The corrections necessary without these precautions would have been of the same order of magnitude as the measured fluxes [*Hargreaves et al.,* this issue]. As indicated in Figure 1, a reflux scheme was applied to the Perma Pure dryer by using the expanded, dried air at the exit of the measurement cell to take up the water vapor from the air sampled at ambient pressure. Dew point measurements indicated a suppression of water vapor concentration by a factor of 60 for the two-stage device, meeting the manufacturer's specifications of a factor $>$ 7.1 per stage.

The damping of temperature fluctuations within the inlet tube can be characterized by the normalized mean temperature

$$\theta_m = \frac{T_0 - T}{T_0 - T_e},$$

T_0, T_e, and T being the wall, entrance, and exit temperatures, respectively. The functional dependence of θ_m on the dimensionless tube length

$$x^+ = \frac{x}{r_0\, Re\, Pr},$$

with tube length x and radius r_0, Reynolds number Re, Prandtl number $Pr = 0.7$ for air, is given by

$$\theta_m = \exp(-2\, Nu_m\, x^+),$$

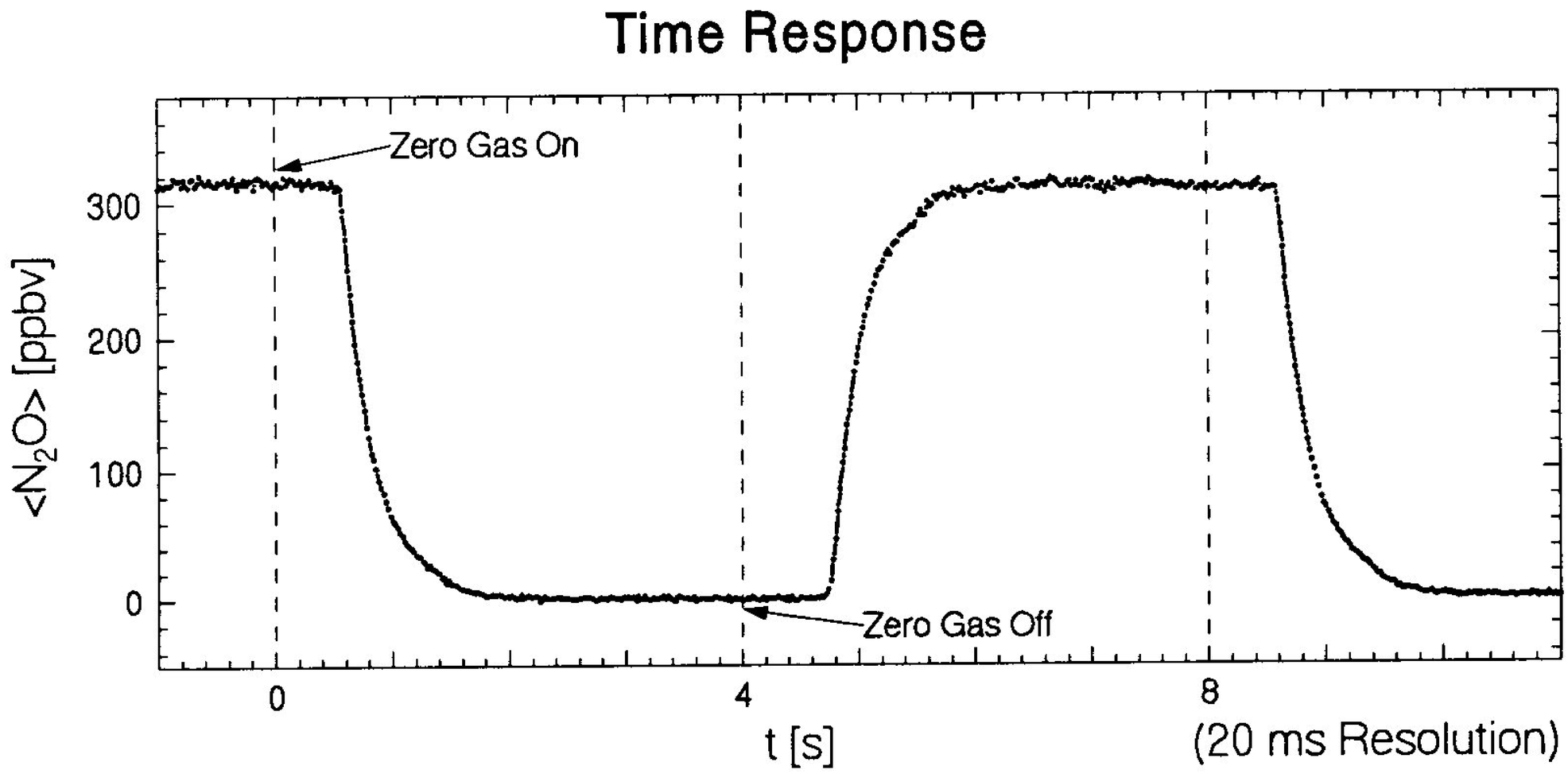

Figure 2. Time response measurement of the instrumental setup. Valve V3 was toggled at 4-s intervals to purge the system with nitrogen, while the concentration was recorded at 50-Hz rate.

where Nu_m (mean Nusselt number) determines the exponential extinction of temperature fluctuations [*Kays and Crawford,* 1980]. In the case of laminar flow, Nu_m itself depends on x^+, approaching 3.7 in the limit of infinitive tube length. For turbulent gas flow however, Nu_m depends solely on the Prantdl and Reynolds numbers and is well approximated by

$$Nu_m = 0.022\, Pr^{0.5}\, Re^{0.8}.$$

Experimental flow conditions lead to $Nu_m = 42.9$, and the inlet $x^+ = 0.33$ was more than 6 times greater than the value $x^+ = 0.054$ needed for a $\theta_m = 0.01$ (i. e., a factor of 100 in suppression of temperature fluctuations). This analysis reveals that turbulent flow conditions in the transfer tube equilibrate the gas much more efficiently to wall temperature than the laminar case [*Leuning and Moncrieff,* 1990]. The same flow conditions however preserve the concentration fluctuations for a constituent with neglectable wall interaction.

3. Tunable Diode Laser Instrument

In tunable diode laser spectroscopy, highly specific mid-infrared trace gas absorptions arising from fundamental rovibrational molecular transitions are monitored using solid state tunable lead salt lasers. These narrowband light sources resolve single lines of the absorption bands for many trace gases at reduced pressure, preventing cross sensitivity to other species. Their high spectral brightness permits fast and sensitive determination of the target trace gas concentration. Tuning of the laser emission wavelength to the selected absorption line is accomplished by the appropriate setting of laser temperature and current, while small variations in the laser current (ramp) serve for scanning the emission across the line [*Schiff et al.,* 1987]. Tunable diode laser spectroscopy has been successfully applied recently for flux measurements of carbon monoxide and methane [*Ritter et al.,* 1992].

The schematic setup of the instrument developed for this study is given in Figure 3. A laser diode controller stabilizes the laser temperature in the range 90, . . . , 130 K with millikelvin precision and provides laser current with ramp modulation under computer control. The major fraction (95%) of the laser light is focused into a multipass White cell [*White,* 1976; *Roths,* 1992] with an optical path of 45.9 m in a 0.45-m base length. The remaining laser power traverses a reference cell containing N_2O at the same pressure as in the sample cell but at high concentration. The resulting signal serves to monitor and correct for long-term drifts in the laser emission wavelength arising from the limited stability of the temperature control circuit (line locking). Calibration of the instrument is achieved by purging the White cell with standard gas of known N_2O mixing ratio at half-hour intervals.

The performance of the instrument was significantly enhanced by the application of the two tone frequency modulation (TTFM) technique [*Cooper and Watjen,* 1986; *Cooper and Warren,* 1987], to our knowledge for the first time in a field experiment. The laser light was frequency modulated at two radio frequencies $\omega_m \pm \Omega/2$ comparable to the absorption line width (ω_m = 280 MHz, Ω = 10 MHz) by adding the corresponding radio frequency (RF) to the laser current (Figure 4) . The RF was produced by suppressed carrier modulation of ω_m at $\Omega/2$ using a mixer. On the detector side, the signal at the beat frequency Ω was monitored by DC conversion using a RF-lock-in amplifier that consisted of a frequency doubler, a phase shifter, a second mixer and a low-pass filter. In the case of no absorption the sidebands produced by the RF modulation in the laser spectrum (see Figure 4) are balanced and no signal is produced at the beat frequency [*Cooper and Warren,* 1987]. As the laser emission is tuned across an absorption feature, the balance is destroyed by differential absorption of the sideband groups and a TTFM signal is generated, as shown in Figure 4. The basic advantage of this technique is to shift the signal detection to the frequency range of Ω = 10 MHz, where there is only a minimal contribution from electronic, detector, and laser noise. Furthermore, due to the high detection frequency, signal changes are established in a few

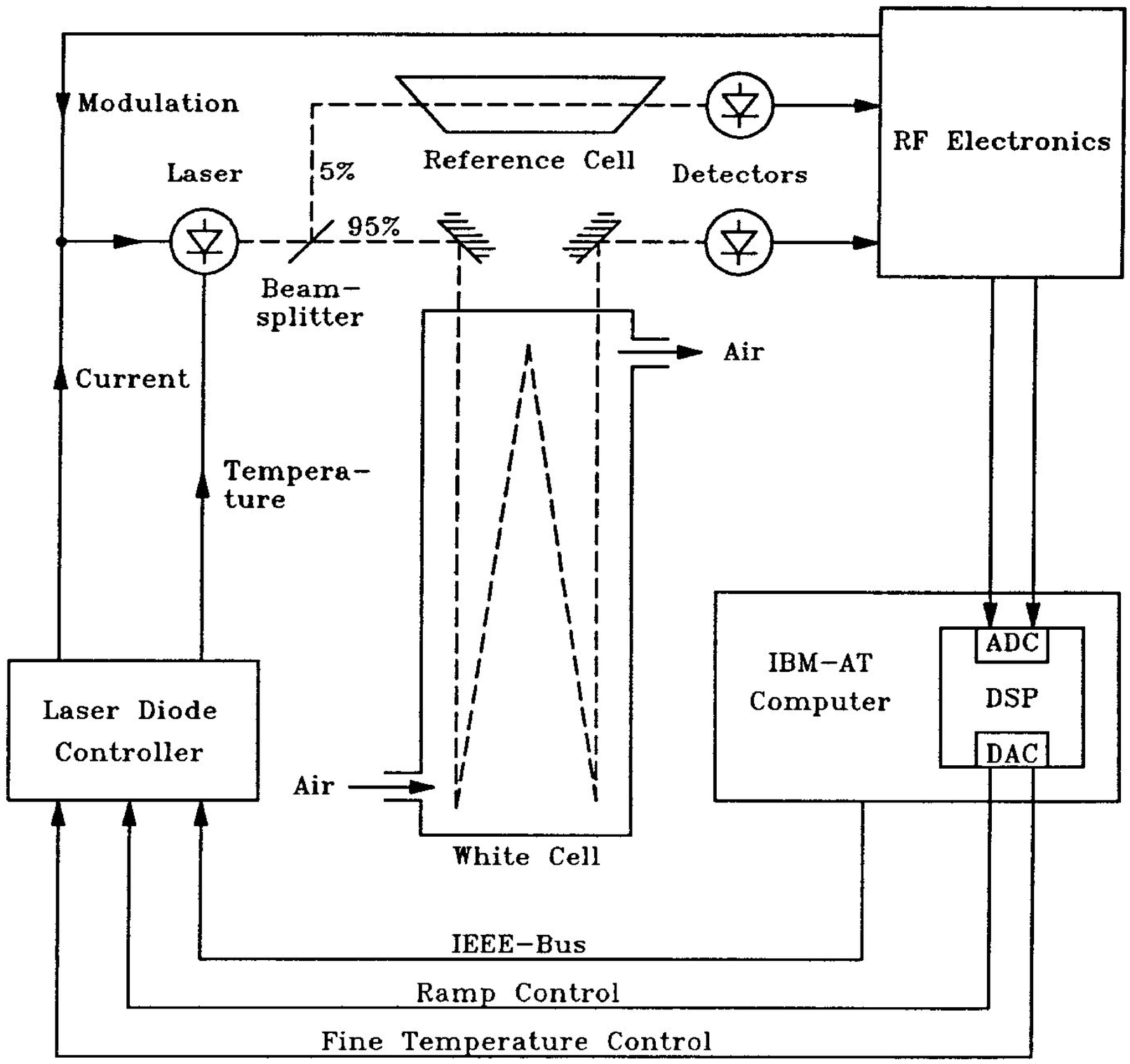

Figure 3. Diagram of the TDL spectrometer used in the study.

microseconds, allowing fast scanning of the laser across the absorption feature (1-ms scan time). For diode lasers, modulation of the driving current produces not only the desired frequency modulation but also an unwanted amplitude modulation [*Cooper and Watjen,* 1986]. In practice, this results in a nonzero background signal at Ω even in the absence of absorption. The low-frequency noise associated with the progression of this background signal during a scan is effectively suppressed by the rapid scanning, further improving instrument performance. Detection limits of 10^{-5} relative absorption for 1-s integration time (corresponding to $\approx$ 140 ppt N_2O mixing ratio) were determined under laboratory conditions. This equals previously reported [*Harris et al.,* 1989] detection limits for field measurements using low-frequency wavelength modulation techniques, but these were obtained with 100– to 1000–fold longer averaging times.

The high data acquisition rate offered by the spectrometer makes it necessary to apply time efficient on-line data handling. The corresponding tasks are distributed between an IBM-AT compatible computer and a digital signal processor (DSP) board connected to the ISA-bus of the AT computer. The AT computer serves as an interface for controlling the instrument and displaying the recorded spectra and calculated N_2O mixing ratios. Concentration data and instrumental parameters are stored on hard disk. The DSP carries out data acquisition, analysis of the TTFM spectra, and generation of the ramp and of the temperature line-locking control signal. The TTFM signal from the White and reference cell detectors are sampled at a rate of 100 kHz by the on-board ADCs synchronously with the ramp DAC output. Spectra containing 100 channels are continuously recorded, resulting in a scan interval of 1 ms. A line-locking procedure is implemented as follows: In parallel to the sampling of the spectra a parabolic fit to the central peak of each reference spectrum indicates the tuning error caused by laser temperature drifts. This error is compensated by shifting each spectrum to align its line center before adding to the average and by modifying the subsequent ramp output. To maintain long-term stability, a suitable PID (proportional–integral–differential) regulation signal is calculated and fed back to the laser temperature control circuit. Spectral averaging time can be software selected appropriate to the measurement requirements (20 ms minimum). To derive the N_2O mixing ratio and its error, a prerecorded calibration spectrum together with a quadratic polynomial to account for background variation is fitted to the averaged spectrum. All calculations are carried out by the DSP in parallel to the continuous data acquisition allowing zero-overhead data analysis.

4. Gradient Measurements

Concentration data for application of the gradient technique were obtained using a spectra integration time of 1 s and by toggling the position of V2 every 20 s. A time delay of 1 s (i. e., one integration period) after switching ensured full gas exchange in the measurement cell. Figure 5 presents

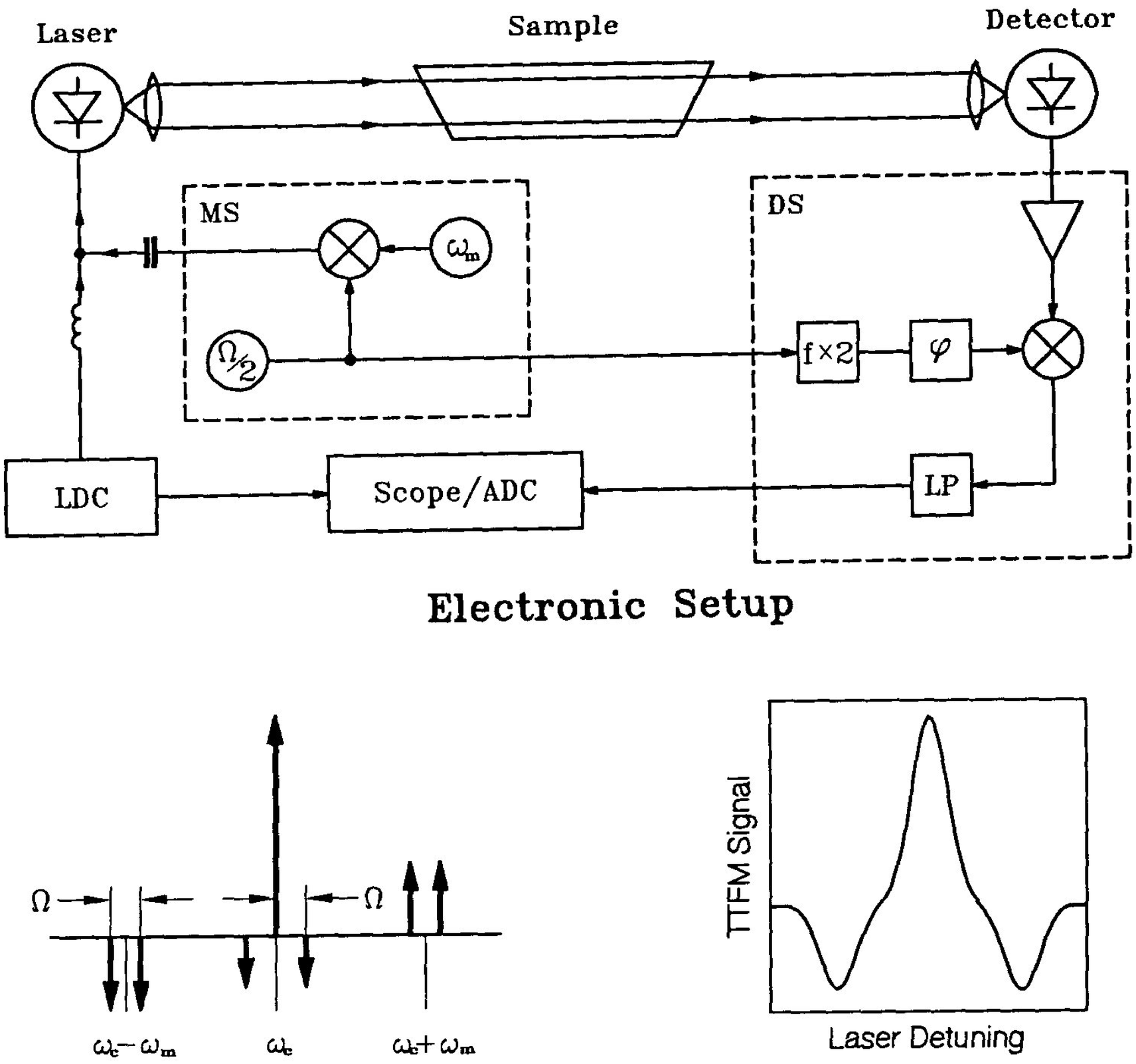

Figure 4. Schematic of the two tone frequency modulation electronics and its sideband and signal generation. MS, modulation section; DS, detection section (RF-lock-in amplifier).

a typical half-hour data set for afternoon mixing conditions (1643, April 11, 1992). Twenty successive samples at each elevation were integrated, the error bars indicating their variability (one standard deviation). The lower part shows the concentration difference normalized to the upper inlet concentration, demonstrating that the instrument is capable of resolving a (statistically significant) difference of less than 1 part per billion by volume (ppbv) at 1-min integration. The normalization became necessary due to slow instrumental drifts at that time which were caused by a grounding problem within the laser temperature control circuit and which were subsequently eliminated. They lead to an apparent 1 % increase of both inlet concentrations during the second half of the measurement interval (Figure 5). Because the instrumental drift during the period needed to determine a concentration difference was small, the normalization reduces the systematic error caused by the drift to a level which is negligible compared to the statistical errors.

Under some nighttime inversion conditions a buildup of up to 50 ppbv N_2O concentration difference was observed, but since turbulent transfer ceases under these conditions, fluxes can be derived from these data only with large uncertainty. Table 1 shows a selection of measurements with the resulting N_2O flux deduced from wind and temperature gradient data [*Hargreaves et al.*, this issue]. The variances of the $\Delta(N_2O)$ means were calculated from the mixing ratio variances during the 20-s measurement times at one elevation. Because the actual mixing ratios at each level are fluctuating during the measurement interval, these variances overestimate the instrument errors. The precision with which the mixing ratio differences could be determined was typically 10 % of the difference for 10-min and 5 % for 30-min averaging periods. This precision leads to uncertainties in the fluxes calculated from the gradients which are small compared to those introduced from other sources, for example, from the derivation of the diffusivity coefficients [*Businger*, 1985].

5. Eddy Correlation Measurements

As discussed, e. g., by *McMillen* [1988], the turbulent vertical mass flux of an atmospheric constituent through an atmospheric layer is directly given by the covariance $\overline{c' w'}$ between the concentration c of the constituent (N_2O) and the vertical component w of the wind vector $\boldsymbol{u} = (u, v, w)$. As usual, the primes denote the quantities' fluctuations and the bar stands for the average over the measurement interval. Similarly, the vertical transfer of horizontal momentum is described by $\overline{\rho u' w'}$ (ρ, air density). Since instrumental delays cause a time lag between wind and concentration measurements, the covariances are evaluated as a function

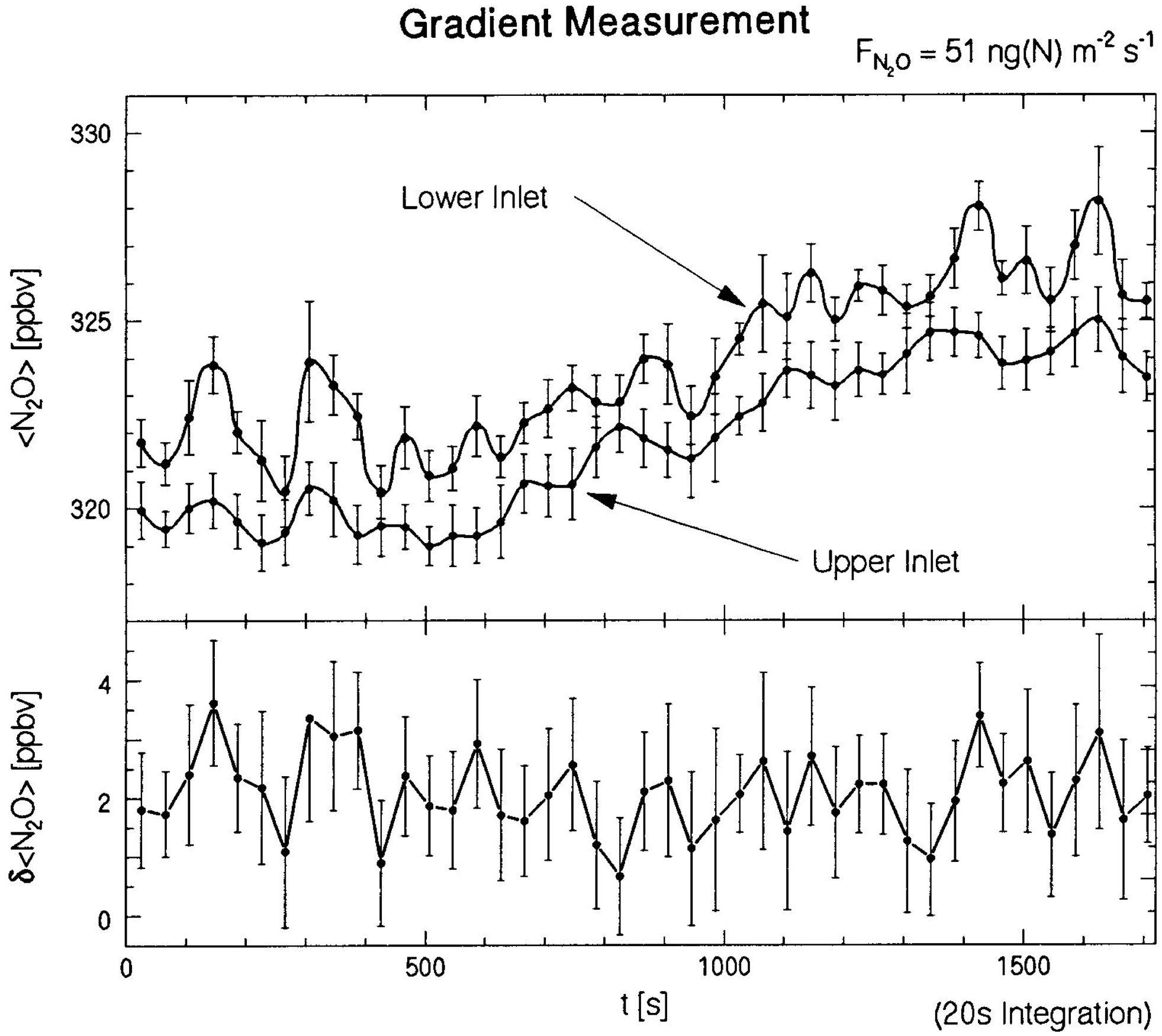

Figure 5. Examples of gradient data acquired at 1-s resolution with V2 switching between the upper and lower inlets. Twenty samples of each inlet are averaged with the error bars indicating the concentration variability during this period. The lower part shows the concentration difference normalized to the upper inlet concentration. A detection limit of $\approx$ 1 ppbv N_2O concentration difference can be estimated at 1-min integration.

of time shift Δt between the samples. Sets of 2^{14} continuous concentration values were acquired at a 10-Hz sampling rate and stored on the TDLAS computer. This resulted in 27.3-min measurement periods and covered a bandwidth of 6.1×10^{-5} Hz to 5 Hz according to the sampling theorem. Wind data from one of two different sonic anemometers (Gill Instruments three-axis research ultrasonic anemometer or Dobbie Instruments PAC–100 sonic anemometer / thermometer system) were logged independently by a second PC, with the start of each measurement interval synchronized. The Dobbie sampling rate could be set to 10 Hz, while for the Gill anemometer it was fixed at 21 Hz. The measurement height was 2.25 m for the Dobbie and 2.75 m for the Gill. The TDLAS inlet point was located close to the respective instrument. The inlet flow due to sampling did not disturb the wind measurements, as verified experimentally.

Data were analyzed off line. The software we developed therefore had to perform the following tasks: scaling the time base of the different data sets, drift compensation, calculating the covariances as a function of Δt, and coordinate rotation to ensure that the vertical wind component lies perpendicular to the shear plane. Time efficient fast Fourier transform

Table 1. Typical N_2O Fluxes Measured With the Gradient Technique

Date	Time	Interval min	$\Delta\langle N_2O\rangle$ ppbv	F_{N_2O} ng N m^{-2} s^{-1}
April 10, 1992	1741	10	4.73 ± 0.46	48
	1754	30	4.49 ± 0.23	44
	2034	30	5.67 ± 0.25	64
	2153	30	$6.3 \cdots 50.4$	$20 \cdots 70$
April 11, 1992	1632	10	2.12 ± 0.28	59
	1643	30	0.79 ± 0.10	51

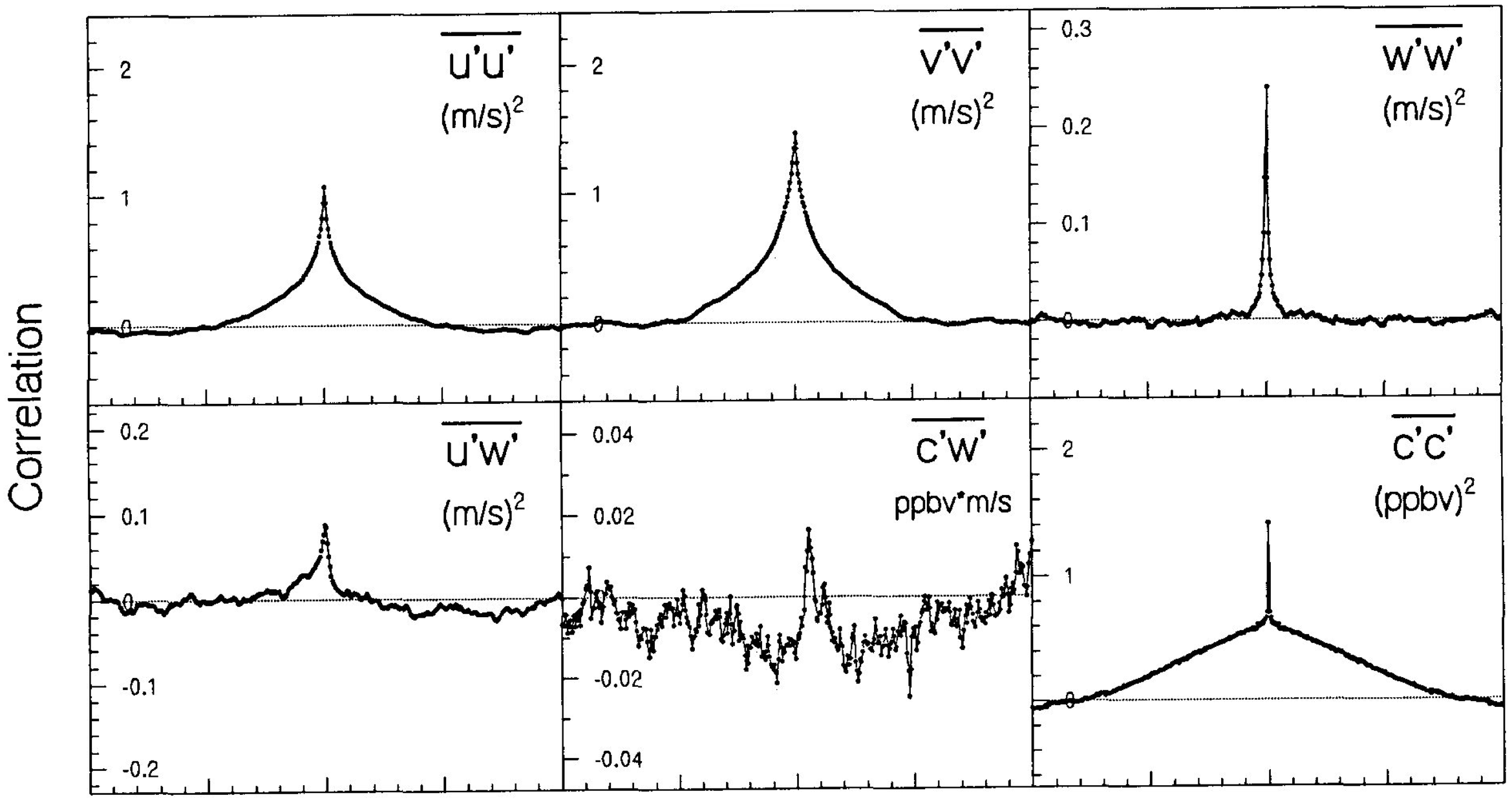

(a) unrotated

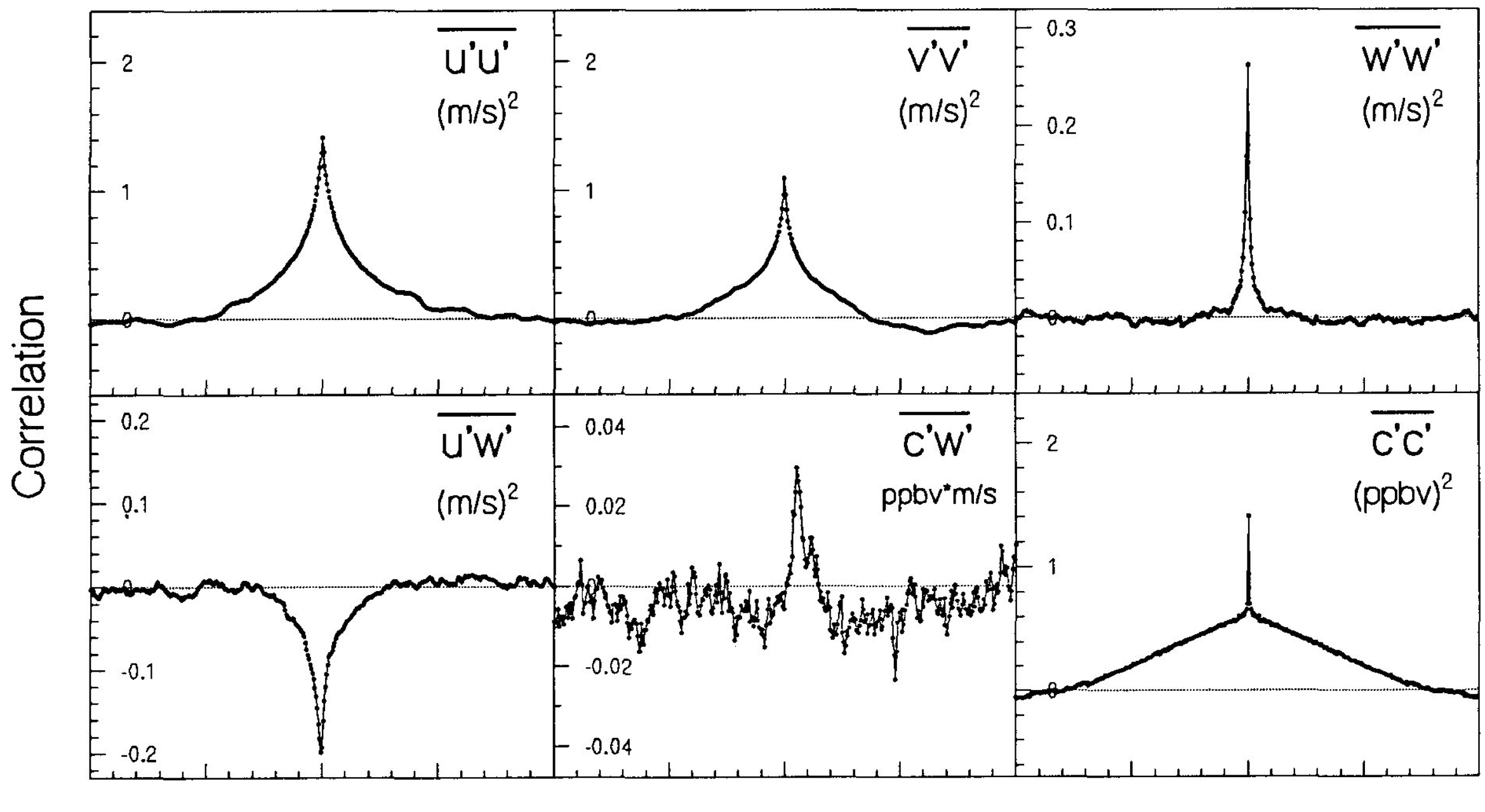

(b) rotated

Figure 6. (a) unrotated and (b) rotated covariances. Wind data were acquired using the Gill anemometer. Rotation reveals downward momentum transfer (u'-w') and suppresses background in the c'-w' covariance. The unusual shape of the c'-c' autocorrelation arises from fetch inhomogeneities.

(FFT) methods were applied for the calculations, which also directly gave information on the frequency power distribution of the wind velocity and of the concentration spectra and their cospectra. Time base scaling was achieved by numerically low-pass filtering the faster wind data and software resampling it at the concentration measurement intervals. This procedure was also necessary for the Dobbie data sets since they proved to have a sampling frequency slightly higher than 10 Hz. In this manner all data were represented by sets of 2^{14} values covering 27.3 min of measurement time. These data sets were subjected to a FFT algorithm and high-pass filtered in the frequency domain for drift compensation. To obtain the covariance between two data sets, the transform of the first was multiplied with the conjugate complex of the second, following the correlation theorem. In the case of identical sets, the result is the power spectral density (PSD).

To compress the further computations, 16 product values were averaged. Inverse FFT finally produced the covariance function in the range of $|\Delta t| \leq 51.2$ s with 0.1-s resolution, containing the desired information.

With this scheme, the six components of the Reynolds stress tensor S ($\overline{u'u'}$, $\overline{v'v'}$, $\overline{w'w'}$, $\overline{u'v'}$, $\overline{u'w'}$, $\overline{v'w'}$) and the three components of the concentration–wind covariance vector $\overline{c'\boldsymbol{u'}}$ were obtained as a function of Δt. Coordinates of this reduced data set were subsequently rotated at three angles to correct for the small errors in the orientation of the anemometers that are inevitable on a field site setup. We followed the algorithm described by *McMillen* [1988]: two angles (θ, ϕ) aligned the rotated u axis with the mean wind direction, the third angle (ψ) around this axis was chosen so as to zero the $\overline{v'w'}$ component of the Reynolds stress tensor near $\Delta t = 0$. This procedure is motivated by the idea that mean vertical transfer of horizontal momentum only occurs in the mean wind direction. The rotation was represented by a 3 × 3-matrix $\mathsf{R} = \mathsf{R}(\theta, \phi, \psi)$. Vector properties (such as $\overline{c'\boldsymbol{u'}}$) were rotated by calculating $\mathsf{R}\,\overline{c'\boldsymbol{u'}}$, and the Reynold stress tensor S was rotated according to $\mathsf{R}^{\mathsf{T}}\mathsf{S}\mathsf{R}$. The resulting values for θ (0°, . . . , 4°) and ψ (-5°, . . . , 5°) agree with the expected alignment errors and indicate that the wind field was not seriously disturbed by the experimental setup.

6. Discussion

Figures 6 to 8 illustrate results of this data treatment. Figure 6 demonstrates the effect of coordinate rotation on a data set whose wind data were acquired using the Gill sonic anemometer. The $\overline{u'w'}$ component of the Reynolds tensor indicates the expected downward transfer of horizontal momentum if the correct coordinate rotation is applied. The rotation also reduces background in the $\overline{c'w'}$ covariance, and from the peak in this figure a N_2O flux of 30 pptv × m/s (37.5 ng N m^{-2} s^{-1}) can be derived. This corresponds to the lowest N_2O flux encountered during the study, and from signal to noise analysis of the covariance function we estimate a detection limit of 6 ng N m^{-2} s^{-1}. A slight asymmetry in the $\overline{u'u'}$ and $\overline{v'v'}$ components with respect to Δt becomes obvious in the rotated data set. This effect can be explained by considering the cylindrical sampling volume of the Gill anemometer which results in different instrumental transfer functions for the horizontal and vertical wind components. Therefore an ideal tensor behavior under coordinate rotation cannot be expected. The consequences of transfer function mixing are very small however as compared to the autocorrelation peaks and do not impede data interpretation. Applied to the Dobbie wind data sets, the same rotation scheme does not reveal a downward momentum transfer, a typical example being shown in Figure 7. This is possibly the result of wind field disturbance by the body of this anemometer which was in the same plane as the ultrasonic transducers, i. e., the sampling volume. The Gill instrument layout seems to be better suited for this kind of analysis.

The remarkable shape of the concentration autocorrelation function shown in these figures is typical for the data set as a whole. The function consists of two contributions with distinct coherence times: the short-time peak on top of the long-time broad background corresponds to the peak in the $\overline{w'w'}$ correlation function, while the broad background itself corresponds to the horizontal wind components' autocorrelation. Correlation between concentration and horizontal air movement should not occur in the case of measurements on an ideal homogeneous fetch, and we conclude that it arises in this case from the inhomogeneity of the present fetch, parts

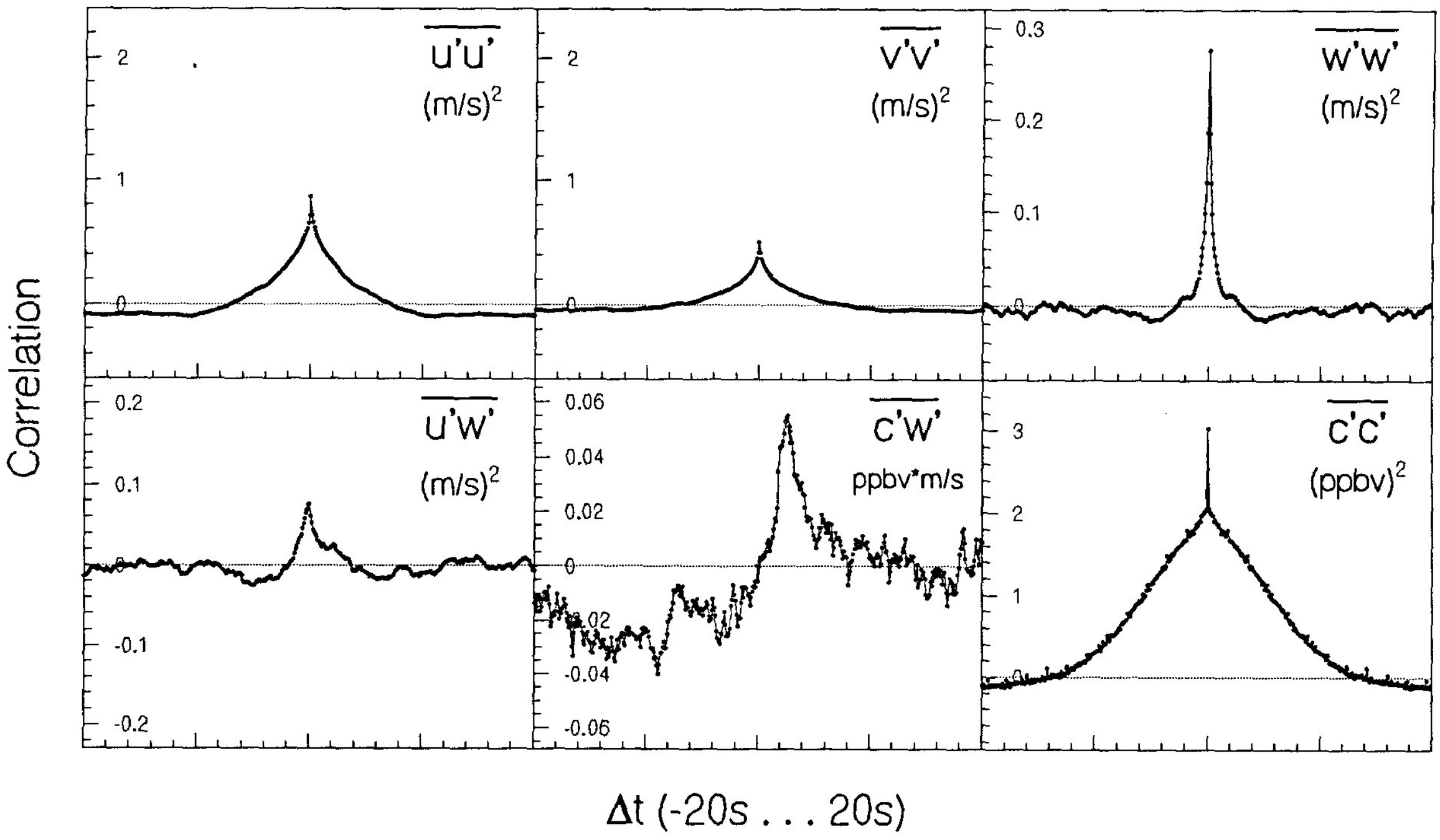

Figure 7. Typical rotated Dobbie data set. Downward transfer of horizontal momentum is not established due to wind field disturbance (u'-w' covariance). The other covariances agree with Figure 4.

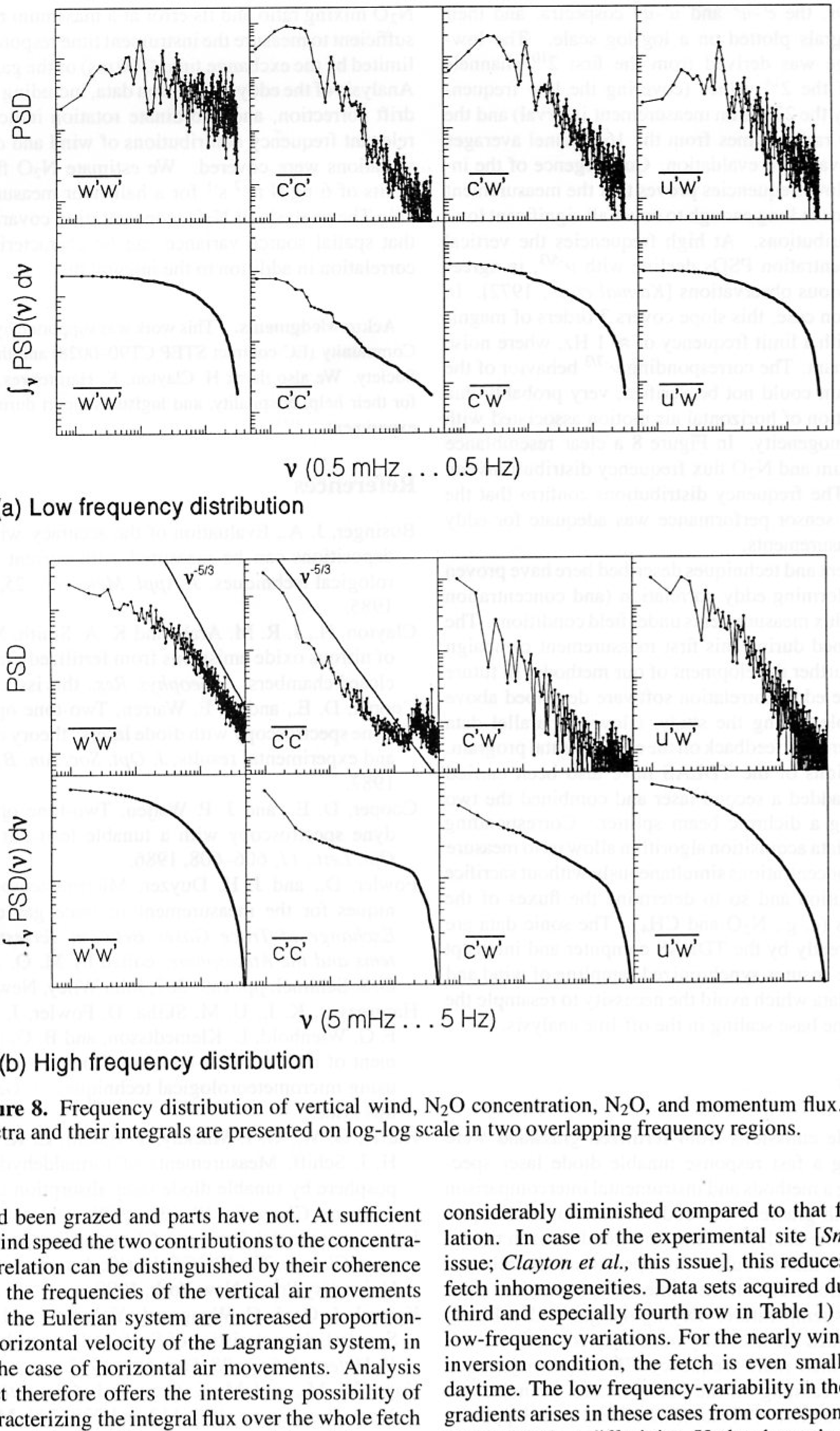

Figure 8. Frequency distribution of vertical wind, N_2O concentration, N_2O, and momentum flux. The spectra and their integrals are presented on log-log scale in two overlapping frequency regions.

of which had been grazed and parts have not. At sufficient horizontal wind speed the two contributions to the concentration autocorrelation can be distinguished by their coherence times, since the frequencies of the vertical air movements measured in the Eulerian system are increased proportionally to the horizontal velocity of the Lagrangian system, in contrast to the case of horizontal air movements. Analysis of this effect therefore offers the interesting possibility of not only characterizing the integral flux over the whole fetch but also its spatial variability by means of the eddy correlation technique. Corresponding low-frequency variation in the gradient data was not observed. Because of the different sampling heights the fetch for the gradient measurements is considerably diminished compared to that for eddy correlation. In case of the experimental site [*Smith et al.*, this issue; *Clayton et al.*, this issue], this reduces the effects of fetch inhomogeneities. Data sets acquired during nighttime (third and especially fourth row in Table 1) exhibit distinct low-frequency variations. For the nearly windless nighttime inversion condition, the fetch is even smaller than during daytime. The low frequency-variability in the concentration gradients arises in these cases from corresponding variations in the turbulent diffusivity. Under these circumstances it is not valid to apply the concentration gradient method for flux derivation.

Figure 8 shows typical frequency (ν) distributions of the

c' and w' PSDs, the c'-w' and u'-w' cospectra, and their frequency integrals plotted on a log-log scale. The low-frequency range was derived from the first 2^{10} channels of the FFTs of the 2^{14} values (covering the low frequencies resolved by the 27.3-min measurement interval) and the high-frequency range comes from the 16-channel averages used for the covariance evaluation. Convergence of the integrals toward low frequencies proves that the measurement interval was chosen long enough to cover all significant low-frequency contributions. At high frequencies the vertical wind and concentration PSDs decline with $\nu^{-5/3}$, in agreement with previous observations [*Kaimal et al.*, 1972]. In the concentration case, this slope covers 3 orders of magnitude in PSD with a limit frequency of $\approx$ 1 Hz, where noise becomes dominant. The corresponding $\nu^{-7/3}$ behavior of the c'-w' cospectrum could not be verified, very probably due to the contribution of horizontal air motion associated with the fetch inhomogeneity. In Figure 8 a clear resemblance of the momentum and N_2O flux frequency distributions can be observed. The frequency distributions confirm that the N_2O and wind sensor performance was adequate for eddy correlation measurements.

The instrument and techniques described here have proven capable of performing eddy correlation (and concentration gradient) N_2O flux measurements under field conditions. The experience gained during this first measurement campaign has led to the further development of our methods. In future experiments the eddy correlation software described above will be available during the study, allowing parallel data analysis and thereby a feedback on the experimental program. Two modifications of the TDLAS have also been carried out. We have added a second laser and combined the two beams by using a dichroic beam splitter. Corresponding changes to the data acquisition algorithm allow us to measure two trace gas concentrations simultaneously without sacrifice temporal resolution and so to determine the fluxes of the two trace gases (e. g., N_2O and CH_4). The sonic data are now logged directly by the TDLAS computer and interrupt driven software ensures synchronized sampling of wind and concentration data which avoid the necessity to resample the data sets for time base scaling in the off-line analysis.

7. Summary

Nitrous oxide emissions from fertilized grassland were measured using a fast response tunable diode laser spectrometer during a methods and instrumental intercomparison campaign. Both gradient and eddy correlation techniques were applied. The analysis of the flow conditions in the intake tube shows that turbulent flow preserved the relevant N_2O concentration fluctuations while at the same time equilibrated the gas temperature. Drying the gas with a Perma Pure dryer avoided the necessity of density corrections.

We implemented radio frequency TTFM in conjunction with fast laser scanning on the field TDLAS for noise and background reduction. A resolution of less than 1 ppbv in N_2O mixing ratio difference was established for a 1 min measurement interval. The on-line zero-overhead spectra analysis algorithm of the instrument was carried out by a digital signal processer and allowed determination of the N_2O mixing ratio and its error at a maximum rate of 50 Hz, sufficient to measure the instrument time response which was limited by the exchange time (200 ms) of the gas sample cell. Analysis of the eddy correlation data, including time-scaling, drift correction, and coordinate rotation indicated that the relevant frequency contributions of wind and concentration variations were covered. We estimate N_2O flux detection limits of 6 ng N m^{-2} s^{-1} for a half-hour measurement interval. The analysis of N_2O concentration covariance reveals that spatial source variance can be characterized by eddy correlation in addition to the integral flux.

Acknowledgments. This work was supported by the European Community (EC contract STEP CT90–0028) and the Max Planck Society. We also thank H. Clayton, K. Hargreaves, and U. Skiba for their help, hospitality, and logistic support during the Stirling experiment.

References

Businger, J. A., Evaluation of the accuracy with which dry depositions can be measured with current micrometeorological techniques, *J. Appl. Meteorol., 25,* 1100–1124, 1985.

Clayton, H., J. R. M. Arah, and K. A. Smith, Measurement of nitrous oxide emissions from fertilized grassland using closed chambers, *J. Geophys. Res.,* this issue.

Cooper, D. E., and R. E. Warren, Two-tone optical heterodyne spectroscopy with diode lasers: theory of line shapes and experimental results, *J. Opt. Soc. Am. B, 4,* 470–480, 1987.

Cooper, D. E., and J. P. Watjen, Two-tone optical heterodyne spectroscopy with a tunable lead-salt diode laser, *Opt. Lett., 11,* 606–608, 1986.

Fowler, D., and J. H. Duyzer, Micrometeorological techniques for the measurement of trace gas exchange, in *Exchange of Trace Gases Between Terrestrial Ecosystems and the Atmosphere,* edited by M. O. Andreae and D. S. Schimel, pp. 189–207, John Wiley, New York, 1989.

Hargreaves, K. J., U. M. Skiba, D. Fowler, J. R. M. Arah, F. G. Wienhold, L. Klemedtsson, and B. Galle, Measurement of nitrous oxide emission from fertilized grassland using micrometeorological techniques, *J. Geophys. Res.,* this issue.

Harris, G. W., G. I. Mackay, T. Iguchi, L. K. Mayne, and H. I. Schiff, Measurements of formaldehyde in the troposphere by tunable diode laser absorption spectroscopy, *J. Atmos. Chem, 8,* 119–137, 1989.

Intergovernmental Panel on Climate Change (IPCC), *Climate Change, The IPCC Scientific Assessment,* Cambridge University Press, New York, 1990.

Kaimal, J. C., J. C. Wyngaard, Y. Izumi, and O. R. Cote, Spectral characteristics of Surface-layer turbulence, *Q. J. R. Meteorol. Soc., 98,* 563–589, 1972.

Kays, W. M., and M. E. Crawford, *Convective Heat and Mass Transfer,* pp. 106–112 and 238–244, McGraw-Hill, New York, 1980.

Lenshow, D. H., and M. R. Raupach, The attenuation of fluctuations in scalar concentrations through sampling tubes, *J. Geophys. Res., 96,* 15,259–15,268, 1991.

Leuning, R., and J. Moncrieff, Eddy covariance CO_2 flux measurements using open- and closed-path CO_2 analysers: corrections for analyser water vapor sensitivity and damping of fluctuations in air sampling tubes, *Boundary Layer Meteorol., 53,* 63–76, 1990.

McMillen, R. T., An eddy correlation technique with extended applicability to non-simple terrain, *Boundary Layer Meteorol., 43,* 213–245, 1988.

Ritter, J. A., J. D. W. Barrick, G. W. Sachse, G. L. Gregory, M. A. Woerner, C. E. Watson, G. F. Hill, and J. E. Collins, Jr., Airborne flux measurements of trace species in an arctic boundary layer, *J. Geophys. Res., 97,* 16,601–16,625, 1992.

Robertson, G. P., Fluxes of nitrous oxide and other nitrogen trace gases from intensively managed landscapes: A global perspective, in Agricultural Ecosystem Effects on Trace Gases and Global Climate Change, *ASA Spec. Publ. 55,* pp. 93–108, Am. Stand. Assoc., 1993.

Roths, J., Development of an airborne laser spectroscopic trace gas sensor and its deployment during the TROPOZ–II aircraft measurement campaign (in German), Ph.D. thesis, pp. 67–70, Fachbereich Phys., Johannes-Gutenberg-Univ., Mainz, Germany, 1992.

Schiff, H. I., G. W. Harris, and G. I. Mackay, Measurement of atmospheric gases by laser absorption spectroscopy, *Am. Chem. Soc. Symp. Ser., 349,* 274–288, 1987.

Smith, K. A., et al., Micrometeorological and chamber methods for measurement of nitrous oxide fluxes between soils and the atmosphere: Overview and conclusion, *J. Geophys. Res.,* this issue.

Webb, E. K., G. I. Pearman, and R. Leuning, Correction of flux measurements for density effects due to heat and water vapor transfer, *Q. J. R. Meteorol. Soc., 106,* 85–100, 1980.

White, J. U., Very long optical paths in air, *J. Opt. Soc. Am., 66,* 411–416, 1976.

H. Frahm and F. G. Wienhold, Air Chemistry Department, Max Planck Institute for Chemistry, P. O. Box 3060, 55020 Mainz, Germany.

G. W. Harris, Centre for Atmospheric Chemistry, York University, 4700 Keele St., North York, Ontario M3J 1P3, Canada.

(Received August 6, 1993; revised November 1, 1993; accepted November 16, 1993.)